BIPOLAR, COLLIMATED OUTBURSTS IN THE PLANETARY NEBULA Hb 4

J. A. LÓPEZ

Instituto de Astronomía, UNAM, Apdo. Postal 877, Ensenada, B.C. 22800, México

AND

W. STEFFEN AND J. MEABURN

Department of Physics and Astronomy, University of Manchester, Oxford Road, Manchester, M13 9PL, England, UK

Received 1997 February 25; accepted 1997 March 24

ABSTRACT

Spatially resolved profiles of the Hα and [N II] 6548, 6584 Å emission lines obtained with the Manchester Echelle Spectrometer combined with the 2.1 m San Pedro Mártir telescope have revealed the remarkable velocity structure in the peculiar planetary nebula Hb 4. The compact, elliptical core shows a moderate splitting in the [N II] 6584 Å line profiles of only $2V_{exp} = 43$ km s^{-1}. However, the detection of high velocities in the nebular line profiles from the elongated, ionized knots protruding symmetrically on both sides of the core give direct evidence of the presence of highly collimated outflows in Hb 4. The line profiles in these symmetric, elongated knots are complex, with radial velocities of ± 150 km s^{-1} with respect to the systemic radial velocity and detached emission regions at further extreme radial velocities.

The long-slit spectra are analyzed with a parameterized description of the emissivity and velocity field of the fast-moving, collimated, ionized flow. The observed profiles are simulated in detail by a model of the emission from a bow shock at the head of the jet followed by a faster high-density component. In Hb 4 we are probably observing the first stages of intermittent outflows that could develop into episodic two-sided jets, as observed in the case of the planetary nebula Fleming 1.

Subject headings: ISM: jets and outflows — ISM: kinematics and dynamics —
planetary nebulae: individual (Hb 4)

1. INTRODUCTION

Hb 4 (PN G003.1+02.9, PK 3+2 1) is a high-excitation, type I planetary nebula (PN) (Costa, De Freitas Pacheco, & De Franca 1996) with a WR nucleus type WC 3-4 (Gorny & Stasynska 1996). Its most striking features must be the elongated, low-ionization knots (Corradi et al. 1996) that protrude from either side of the main body of the nebula. A radio map (Aaquist & Sun 1996) of the nebular core shows some of the characteristics present in the optical morphology. The object is located in the Galactic disk, in the direction of the bulge, with an estimated distance of 2.6 kpc (Van de Steene & Sijlstra 1994). An expansion velocity for the core of $V_{exp} = 23 \pm 2$ km s^{-1} has been determined previously (Robinson, Reay, & Atherton 1982), but no reference to the extended knots has been found in the literature.

There are a few PNs whose morphology is characterized by elongated knots emanating from both sides of a usually compact core, such as K 1-2 (Bond & Livio 1990), suggesting the presence of " straight " symmetric jets. Their appearance is different from those PNs termed " point symmetric " (Schwarz, Corradi, & Melnick 1992), where twisted groups of knots are seen on either side of the nucleus; in some of these cases, their kinematics indicate the presence of bipolar, rotating, episodic jets, or BRETs (e.g., López, Vázquez, & Rodríguez 1995; López et al. 1997; López 1997). The episodic nature of the collimated outflows in PNs has become a seemingly distinctive characteristic in these cases. A clear example is found in the PN Fleming 1 (López, Roth, & Tapia 1993; López, Meaburn, & Palmer 1993; Palmer et al. 1996), where well-developed collimated outflows of a seemingly episodic or intermittent nature are observed.

The interpretation of these phenomena has been presented by several authors from different perspectives. For example, Cliffe et al. (1995) have produced convincing

three-dimensional models of episodic jets in PNs. Hydrodynamic models (Frank, Balick, & Livio 1996), and models involving toroidal magnetic fields (Różyczka & Franco 1996; García-Segura et al. 1997), have also shown reasonable success in reproducing some of the observed structures. Kinematical information, though, is lacking for many of the important cases, which is obviously a crucial element in the understanding of the origin of these high-speed phenomena.

The results of long-slit, spatially resolved observations over Hb 4 are presented in the present paper; these reveal for the first time its complex kinematical structure, which places it as a new important member in the list of PNs with confirmed high-velocity, symmetric, collimated outflows. The resultant emissivity and velocity field in the line profiles are analyzed in terms of radiative bow shocks and reproduced with a simple geometrical model, taking into account the orientation of the outflow with respect to the observer and the slit position on the flows.

2. OBSERVATIONS AND RESULTS

The kinematical observations were obtained with the Manchester Echelle Spectrometer (MES; Meaburn et al. 1984) combined with the f/7.9 focus of the 2.1 m San Pedro Mártir UNAM telescope. This spectrometer has no cross-dispersion. For the present observations, filters of 90 Å bandwidth were used to isolate the 87th order containing the Hα and [N II] 6548, 6584 Å nebular emission lines.

A Textronik CCD with 1024×1024 24 μm square pixels was the detector. Two times binning was employed in both the spatial and spectral dimensions. Consequently, 512 increments, each 0″.60 long, gave a total projected slit length of 5″.12 on the sky. " Seeing " varied between 1″ and 2″ during these observations. The 150 μm wide ($\equiv 10$ km s^{-1} and 1″.9) slit was always oriented east-west. The east/west slit positions, slits 1, 2, and 3, where profiles of the Hα and
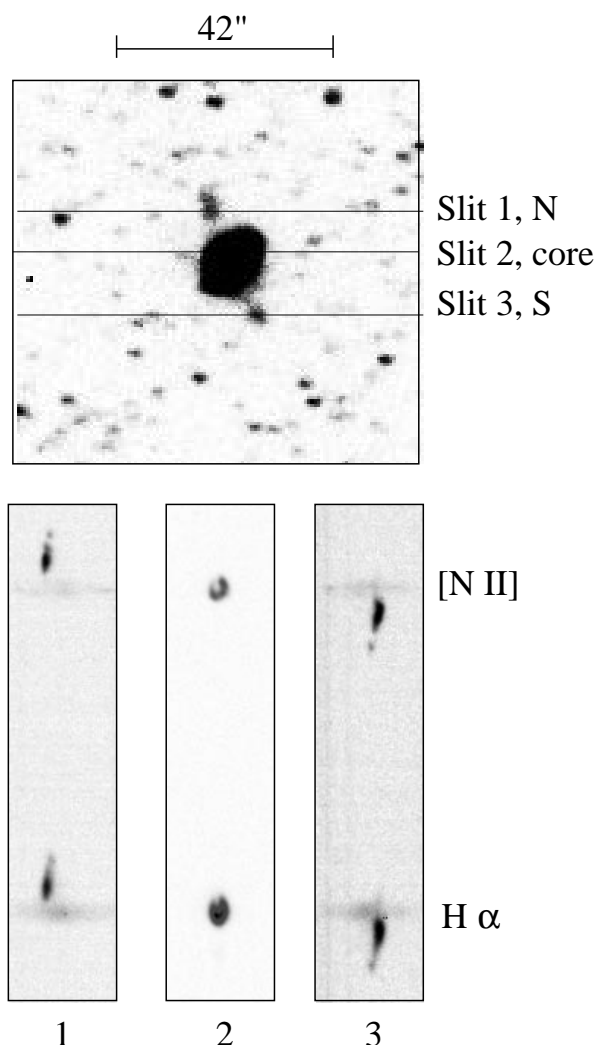
42"

Slit 1, N
Slit 2, core
Slit 3, S

[N II]

H α

1   2   3

FIG. 1.—The long-slit positions (slits 1–3) are marked against the Hα + [N II] 6584 Å image of Hb 4 taken in the direct imaging mode of MES. Gray-scale representations of the position-velocity arrays of the Hα and [N II] 6584 Å profiles along slits 1, 2, and 3 are also shown.

[N II] 6548, 6584 Å lines were obtained, are shown in Figure 1 against an image of Hb 4 taken through the same filter in the imaging mode of MES. These positions intersect the northern elongated knot, the core, and the southern elongated knot, respectively. Gray-scale representations of the position-velocity (pv) arrays containing the Hα and [N II] 6584 Å profiles for the three slit positions are shown also in Figure 1. The angular width of these arrays is equal to the scale mark that appears on top of the image. The slit positions are particularly well known, for the insertion of a plane mirror into the beam before the echelle grating of MES permits an image to be taken of the slit against that of the field being observed (see Meaburn et al. 1984). Integrations of 1800 s duration were obtained for the slit positions over the elongated knots and 60 s for the bright core. Each was followed by a calibration spectrum of a Th/Ar arc. A continuous tungsten spectrum was also obtained to compensate for the variations in sensitivity over the echelle order. The spectra were wavelength calibrated to an accuracy of ± 1 km s^{-1}.

The individual pv arrays for the line profiles corresponding to the northern and southern elongated knots are pre-

sented with logarithmic gray scale in Figures 2 and 3 for Hα and [N II] 6584 Å, respectively. The heliocentric radial velocity (V_{HEL}) scale is marked on the left-hand sides and compared with $V_{HEL} - V_{SYS}$ on the right-hand sides of Figures 2 and 3. Here, the systemic heliocentric radial velocity is measured as $V_{SYS} = -58.9$ km s^{-1}, which is in very good agreement with a previously published value (Kohoutek & Pauls 1995). All velocities hereafter in the text refer to the radial $V_{HEL} - V_{SYS}$ scale, since this indicates straightforwardly the magnitude of the bipolar outflows with respect to the reference frame of the nebula itself. The width of the arrays (42") is the same as that marked in Figure 1. Notice that the 6" angular width of the profiles is resolved.

3. THE KINEMATICS OF HB 4

The line profiles from slit 2 (Fig. 1) indicate that the core of Hb 4 consists of an expanding shell where the splitting of the [N II] 6584 Å line profile reaches $2V_{exp} = 43$ km s^{-1}, to give an expansion velocity of $V_{exp} \simeq 21.5$ km s^{-1}, which is moderate for PNs. However, high-velocity localized outflows are revealed in the line profiles corresponding to slits 1 and 3 (see Figs. 1–3).

The pv arrays of Hα line profiles from the northern (N) and southern (S) elongated knots (slits 1 and 3 and shown in Fig. 2) have intensity maxima at $V_{HEL} - V_{SYS} = +74$ km s^{-1} (N) and -49 km s^{-1} (S) with extreme values of ± 160 km s^{-1}, respectively.

For the corresponding pv arrays of [N II] 6584 Å line profiles, shown in Figure 3, intensity maxima are found at $V_{HEL} - V_{SYS} = +73$ km s^{-1} (N) and -70 km s^{-1} (S). Furthermore, at extreme radial velocities for both northern and southern knots, fainter maxima are clearly resolved at $V_{HEL} - V_{SYS} = +150$ km s^{-1} (N) and -175 km s^{-1} (S), respectively, detached from the main bright component.

The north and south elongated knots are well-collimated structures, with length-to-width ratios of ~ 3. Also, their distinct nature is reflected in the differences between the Hα/[N II] 6584 Å line intensity ratios for the knots, ~ 1.10 (N) and ~ 1.20 (S), in contrast with a value of 3.29 for the core, as expected for a photoionized region.

Note that the major axis of the main elliptical shell seems nearly perpendicular to the bipolar outflows, though these are not perfectly aligned with respect to each other. The direction away from the central star of the northern knot is tilted by $\sim 5°$ with respect to that of the southern one in the image in Figure 1.

The kinematics and morphologies of these two elongated knots strongly suggest their generation by jets or "bullets" from the central star.

3.1. A Geometric Bow-Shock Model

The kinematics, morphology, and line ratios of the elongated knots to the north and south of the main body of Hb 4 indicate that they represent high-velocity, collimated outflows emerging from the core of this PN in a nearly symmetric fashion. In the detailed analysis of their line profiles, it therefore seems reasonable to assume the presence of jets with radiative bow shocks at their leading fronts in these structures. We notice that the line profiles from these outflows show intensity maxima located toward mid velocities, with a fainter broad pedestal and seemingly detached regions of emission at the most extreme positive and negative radial velocities observed. In particular, a peculiar cur-
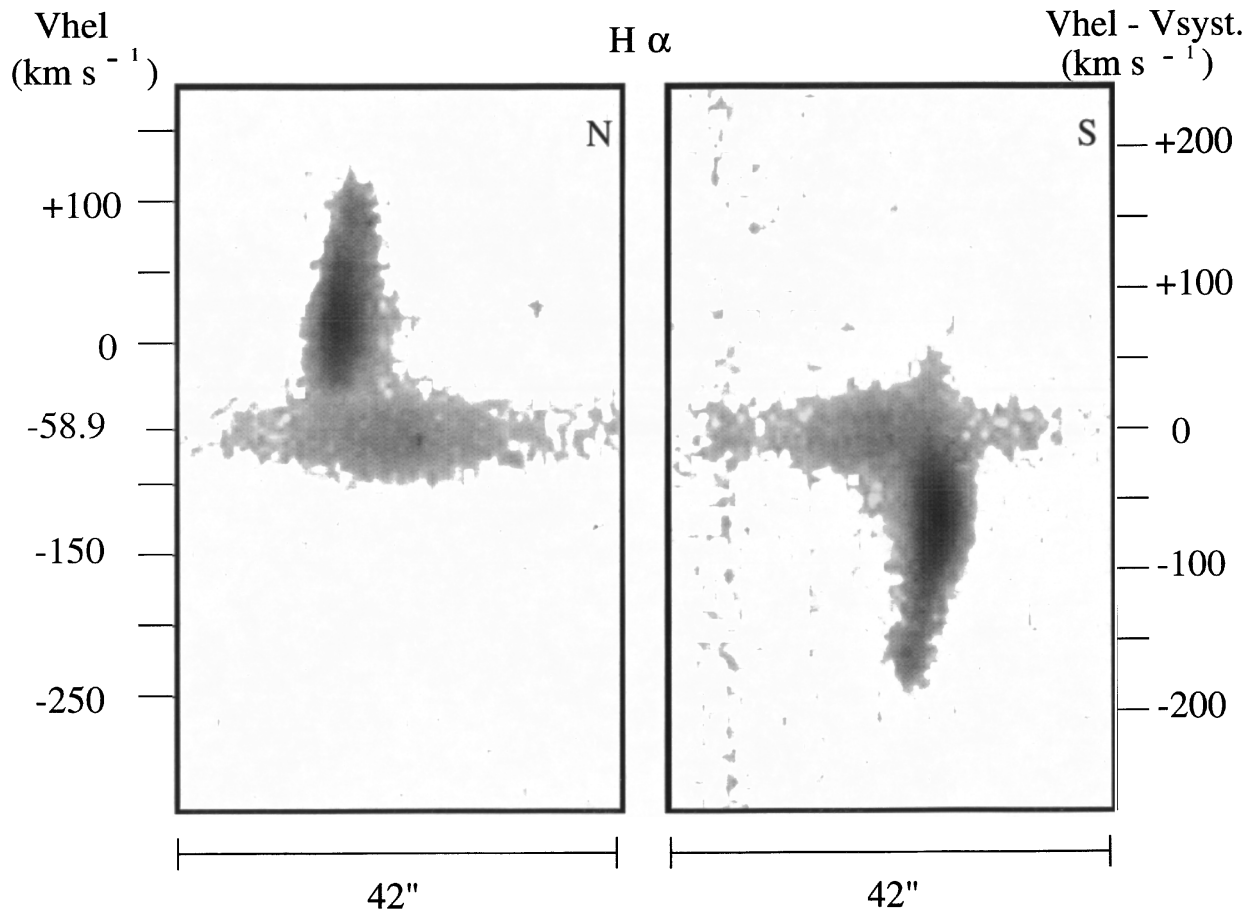
FIG. 2.—Gray-scale representations of position-velocity arrays for the Hα line profiles from slits 1 (N) and 3 (S). The heliocentric radial velocity scale is marked on the left-hand side, and a $V_{\rm HEL} - V_{\rm SYS}$ scale is marked on the right-hand side. The measured heliocentric systemic radial velocity $V_{\rm SYS} = -58.9$ km s^{-1}. The width of the arrays are equal to the 42″ marked in Fig. 1.

vature or tilt in the line profiles is apparent in the pv space.

In order to model the peculiar characteristics of the line profiles observed in the outflows of Hb 4 shown in Figures 2 and 3, a simple geometric approach is used for their description to explore whether or not a radiative bow shock similar to those found in Herbig-Haro (HH) objects (Hartigan, Raymond, & Hartmann 1987, hereafter HRH) is a viable model.

The most extreme approaching and receding features in the jet spectra appear not to be part of the bow shocks themselves. Since they are present in both outflows at similar distance from the nebular core, it is unlikely that they are part of a clumpy structure within the bow shocks. An alternative is that they could be fast-moving knots within the jet driving the bow shocks. These knots are therefore modeled separately as discrete components at a distance z_c from the apex of the bow shocks with flow speeds v_c, radius r_c, thickness d_c, and emissivity ϵ_c (Fig. 4).

In the following we use some results from HRH to narrow down the parameter space for the simulations of the pv diagrams. If the bow shock emission is detected sufficiently far downstream, then the speed and orientation of the bow shock can be estimated directly from the FWZI and the minimum ($v_{\rm min}$) and maximum ($v_{\rm max}$) radial velocities of a low-ionization spectral line profile (HRH). From the observed knot sizes (3″) and seeing conditions (1″–2″), we conclude that at least partial emission from the full knot is included in the spectral observation. We find that $v_{\rm min} \approx 0$

± 20 km s^{-1} and $v_{\rm max} \approx 120 \pm 20$ km s^{-1} for the low-ionization Hα line. The observation that $|v_{\rm min}| \ll |v_{\rm max}|$ implies that the angle θ between the axis of the bow shock and the observer's line of sight has to be rather small ($\theta < 45°$) and that the bow-shock velocity $v_b \geq v_{\rm max}$ (HRH).

An estimated lower limit to θ can be found from the measured projected distance d_{bp} of the bow shock from the center of the PN, its velocity v_b, and the age t_e of the PN. The age of the PN is estimated from its radius $r_e = 1.6 \times 10^{12}$ km and expansion velocity $V_{\rm exp} = 21.5$ km s^{-1}, with the result $t_e = r_e/V_{\rm exp} \approx 2300$ yr. The age t_b of the bow shock is larger than the projected distance from the PN shell $d_{bp} - r_e$ divided by its speed v_b: $t_b > (d_{bp} - r_e)/v_b = 525$ yr. Assuming that the collimated outflows are younger than the PN, we have $\sin \theta = (d_{bp} - r_e)/(d_b - r_e) > t_b/t_e \approx 0.27$, where d_b is the deprojected distance from the center of the PN. Consequently, we find the viewing angle in the range $45° \geq \theta \geq 16°$.

The intersection angle between the slit and the projected bow-shock axis, assumed to be the line joining the center of the PN and the outflow, has been determined from the image in Figure 1. The slit position is oriented east-west, and the position angles observed for the elongated knots to the north and south of the PN are 20° and 205°, respectively. The simulations are concentrated on the southern outflow but are equally valid by symmetry, within the uncertainties, for both cases.

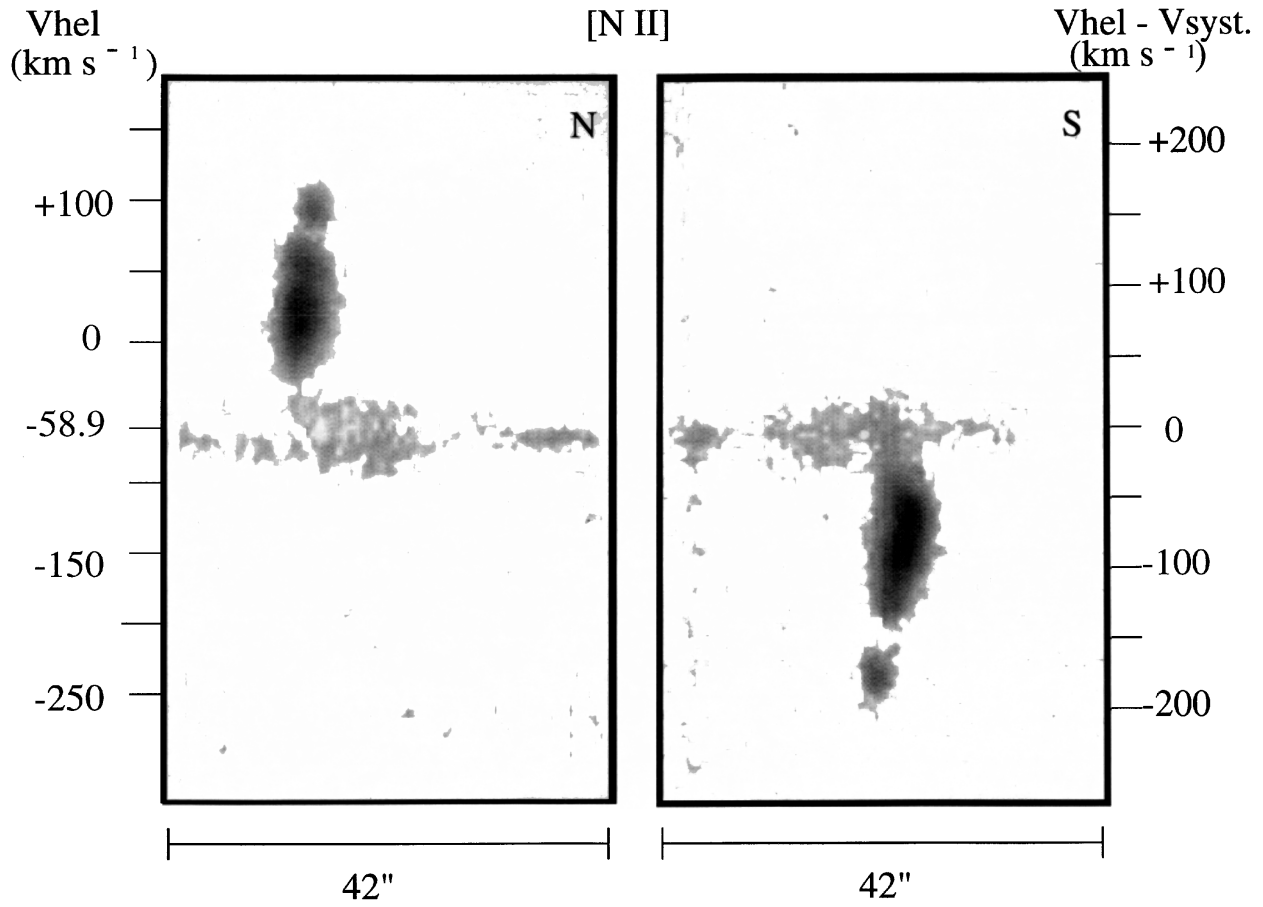The shape of the bow shock is described following the

Fig. 3.—Same as Fig. 2, but for the [N II] 6584 Å profiles

formalism described by Henney (1996) in the axisymmetric case. The shape is given by the radius $r(z)$ as a function of distance z from the apex:

$$r(z) = (\psi + 1)z^{1/(\psi + 1)} , \qquad (1)$$

where ψ is a constant determining the "bluntness" of the bow shock's nose. The bow shock is assumed to be radiative such that, in the velocity frame of the bow shock, the post-shock velocity component of the gas perpendicular to the bow-shock surface is negligible. The velocity of the shocked gas in the rest frame of the environment is then given by (Henney 1996)

$$\mathbf{v} = \{v_r, v_z\} = \frac{v_b}{1 + g^2} \{g, 1\} , \qquad (2)$$

where v_b is the bow-shock speed and $g = z^\psi$. For the present purpose, it is sufficient to use a simple analytical description of the emissivity distribution in a thin sheet as a function $\epsilon_{(z)}$ of distance z from the apex. This function is a Gaussian-type function of arbitrary order:

$$\epsilon = \epsilon_0 \exp\left(-\frac{z^\xi}{2\xi(\kappa w)^\xi}\right), \qquad (3)$$

where w is the distance at which the emissivity decreases to approximately $\epsilon_0/2$ and $\kappa = 0.849$. Only relative intensities are considered; hence, we set $\epsilon_0 = 1$. The parameter ξ gives control over the sharpness of the decline of the emission. Since the spatial extent of the [N II] 6584 Å emission is smaller and rather sharply edged as compared with that of Hα (see Fig. 2), the cutoff position of [N II] 6584 Å appears to lie within the slit opening. This limits the parameter w to values smaller than the slit size of $1''.9$.

For the simulation of the long-slit spectra, we use the modeling code SHAPE described in Steffen, Holloway, & Pedlar (1996). It allows the calculation of long-slit spectra for arbitrary orientation of a given emissivity and flow distribution in space on a regular three-dimensional Cartesian grid. For the simulations in the present paper, a grid size of 141 cells in each direction is used, corresponding to $14''$. The
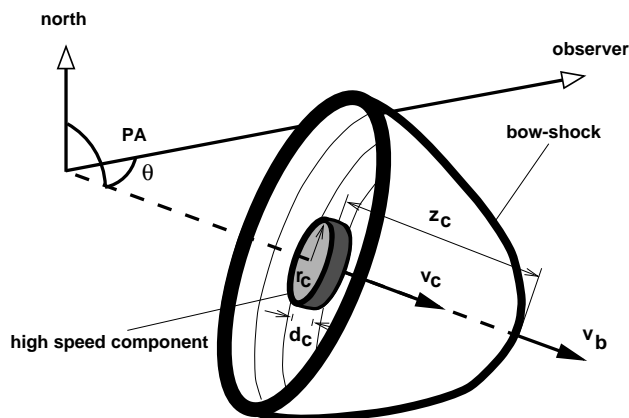

Fig. 4.—Schematic representation of the bow-shock plus high-speed component for the outflows in Hb 4 (for the southern knot). The relevant model parameters are indicated.
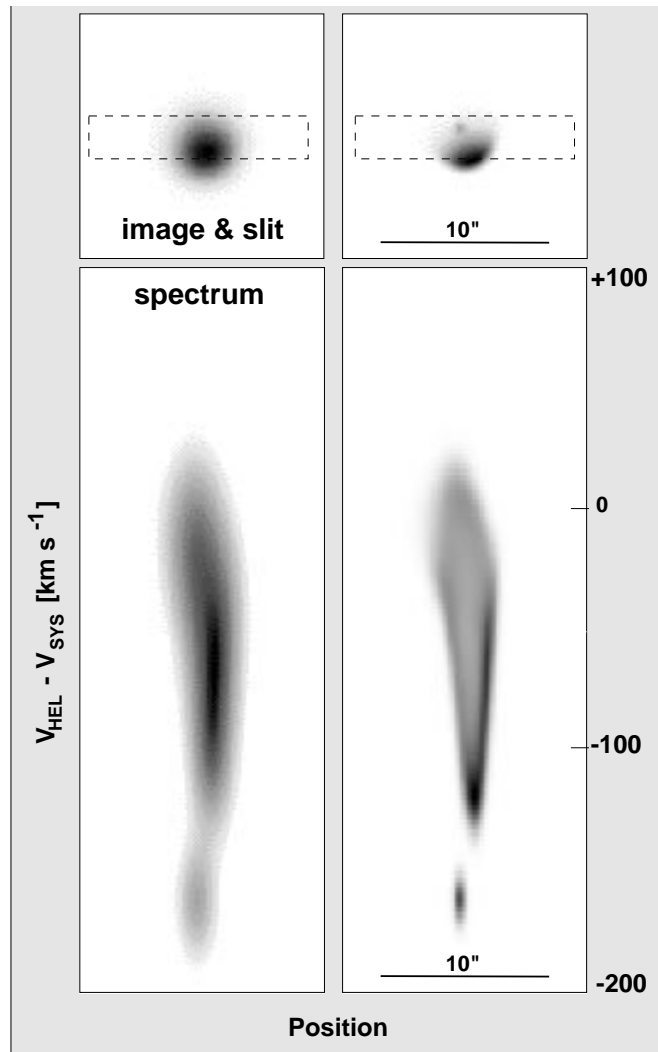
FIG. 5.—Representative simulated images (*top*) and pv diagrams (*bottom*) for the southern knot are shown at different resolutions. On the left-hand side, the simulated seeing and velocity resolution are 1″.9 and 30 km s^{-1}, respectively, representative for the observing conditions. To make the underlying image and spectral structure visible in more detail, the same spectra have been represented with values of 0″.5 and 15 km s^{-1} for the respective resolutions in space and velocity. The slit coverage is marked with a dashed box.

spectrum consists of 141 velocity channels ranging from -100 to $+200$ km s^{-1}.

3.2. *Results of the Model*

Representative model spectra and images are presented in Figure 5 with a simulated seeing of 1″.9 (matching the seeing of the observations; *left*) and a 5 times higher resolution (to see the underlying detailed structure of the model; *right*). The parameters used in the simulation for the simulated pv diagrams shown in Figure 5 are listed in Table 1. Length scales here are given in arcseconds since the model results are not determined by any given true length scale. These model spectra should be compared with the observed spectra in Figures 2 and 3.

The velocity extent of the simulated bow-shock spectrum depends mainly on the orientation with respect to the observer and the observing slit, as well as its advance speed in the ambient medium. These have been determined from

TABLE 1
MODEL PARAMETERS

Parameter	Value
Orientation	
Viewing angle: θ (deg)	40
Position angle: PA (deg)	205
Bow Shock	
Velocity: v_b (km s^{-1})	170
Bluntness parameter: ψ	1.5
Emission half-width: w (arcsec)......	0.8
Emission exponent: ξ.................	0.8
Emissivity: ϵ_b (relative units).........	1
Secondary Knot	
Velocity: v_c (km s^{-1})	220
Radius: r_c (arcsec).....................	0.2
Thickness: d_c (arcsec)	0.3
Apex distance: z_c (arcsec)	0.5
Emissivity: ϵ_c (relative units).........	70

the observed spectra to within a narrow range, assuming the properties of the radiative bow-shock model by HRH. Within this parameter range, the simulation reproduces the observed radial velocity spread.

Assuming that the highest emissivity is located at the apex of the bow shock, the observed position of the maximum in the pv diagram is achieved only if the observing slit does not fully cover the apex region of the bow shock, i.e., the bright apex is down-weighted by at least temporal exclusion by seeing motion during the observation. Otherwise, the maximum would be found at the extreme velocity end for the parameter range determined in the previous section. The peak brightness of the simulated spectrum depends then quite strongly on the seeing and the exact position of the slit. The reason for this is that the effect of the seeing is an integration over a given spatial region. The simulated high-resolution spectrum displayed in Figure 5 shows that the spectrum is roughly of triangular shape. Consequently, the maximum integrated intensity varies with resolution if it is partially resolved in the spatial direction. Under these conditions, the observed spectra are very well reproduced by our simple bow-shock plus high-speed knot model.

3.3. *The Dynamical Nature of the High-Speed Knots*

We consider three possible dynamical explanations for the extreme high-speed knots in Hb 4. The first two possibilities are backward shocks propagating into a high-density bullet or a high-density jet driving the bow shocks. In both of these cases, however, we would obtain less extreme radial velocities for the emitting shocked gas as compared with the bow–shock speed. Hence, we exclude this possibility as the origin of the high-speed knots. More likely, the high-speed emission knots originate from fast, high-density regions before they pass the Mach shock associated with the bow shock of a jet. Multiple mass ejections over a short period could also result in higher advance speeds of the ejections following the first outburst, because they would propagate through a medium cleared by the leading bow shock. A further possibility is that they are internal working surfaces of episodic or variable velocity jets, similar to those studied by Biro & Raga (1994). The

morphological appearance of the emission maps of the region near the jet head derived by Biro & Raga (1994) are strikingly similar to our simulated high-resolution image (Fig. 5). The internal working surfaces propagate faster than the preceding bow shocks and could explain our observations. More detailed observations and theoretical modeling will be required to decide between the several possibilities for the nature of the extreme high-speed knots in Hb 4.

4. CONCLUSIONS

The north and south elongated knots in Hb 4 are well-collimated structures, with length-to-width ratios of ~ 3. It is unlikely that the expanding shell surrounding the core could be responsible for this degree of collimation, for more typical bipolar lobes would be expected in this case. The elongated structures associated with these high-velocity flows are more likely manifestations of polar outflows being generated close to the stellar surface. The distinct nature of these elongated knots is also reflected in the Hα/[N II] 6584 Å relative line flux ratios between these structures and the core, with values of ~ 1.10 and ~ 1.20 for the integrated spectra of the northern and southern jets, respectively, and 3.29 for the core, the latter corresponding closely to the expected value of a photoionized region.

The major axis of the main elliptical shell seems to be perpendicular to the bipolar outflows, though these are not perfectly aligned with respect to each other. The northern knot is off by $\sim 5°$ with respect to the axis defined by the southern counterpart, as if a torque or warping from the collimating structure had taken place. Such a possibility has been recently shown to be feasible by Livio & Pringle (1996) in some cases of two-sided jets in planetary nebulae.

The position-velocity diagrams of the elongated knots are reproduced well by a simple geometric bow-shock model plus a high-speed component. The success of the simulations in replicating the observed line profiles supports the interpretation of the elongated knots as radiative bow shocks followed by a faster high-density component, which might be the result of a short-lived episodic ejection event. Thus, in Hb 4 we are probably observing the first stages of intermittent outflows that could develop into episodic two-sided jets, as observed, for example, in the case of the planetary nebula Fleming 1.

Hb 4 joins a small but growing and important group of planetary nebulae where collimated, bipolar episodic ejections of high velocity have been observed and that is modifying the traditional views of PN shaping and evolution.

REFERENCES

Aaquist, O. B., & Sun, K. 1996, ApJ, 462, 813
Biro, S., & Raga, A. C. 1994, ApJ, 434, 221
Bond, H. E., & Livio, M. 1990, ApJ, 355, 568
Cliffe, J. E., Frank, A., Livio, M., & Jones, T. W. 1995, ApJ, 447, L49
Corradi, R. L. M., Manso, R., Mampaso, A., & Schwarz, H. E. 1996, A&A, 313, 913
Costa, R. D. D., De Freitas Pacheco, J. A., & De Franca, J. A., Jr. 1996, A&A, 313, 924
Frank, A., Balick, B., & Livio, M. 1996, ApJ, 471, L53
García-Segura, G., Langer, N., Różyczka, M., Mac Low, M., & Franco, J. 1997, ApJ, submitted
Gorny, S. K., & Stasinska, G. 1996, A&A, 303, 893
Hartigan, P., Raymond, J., & Hartmann, L. 1987, ApJ, 316, 323
Henney, W. 1996, Rev. Mexicana Astron. Astrophys., 32, 3
Kohoutek, L., & Pauls, R. 1995, A&AS, 111, 493
Livio, M., & Pringle, J. E. 1996, ApJ, 465, L55

López, J. A. 1997, IAU Symp. 180, Planetary Nebulae, ed. H. J. Habing & H. J. G. L. M. Lamers (Dordrecht: Kluwer), in press
López, J. A., Meaburn, J., Bryce, M., & Rodríguez, L. F. 1997, ApJ, 475, 705
López, J. A., Meaburn, J., & Palmer, J. W. 1993, ApJ, 415, L135
López, J. A., Roth, M., & Tapia, M. 1993, A&A, 267, 194
López, J. A., Vázquez, R., & Rodríguez, L. F. 1995, ApJ, 455, L63
Meaburn, J., Blundell, B., Carling, R., Gregory, D. E., Keir, D. F., & Wynne, C. G. 1984, MNRAS, 210, 463
Palmer, J. W., López, J. A., Meaburn, J., & Lloyd, H. M. 1996, A&A, 307, 225
Robinson, G. J., Reay, N. K., & Atherton, P. D. 1982, MNRAS, 199, 649
Różyczka, M., & Franco, J. 1996, ApJ, 469, L127
Schwarz, H. E., Corradi, R. L. M., & Melnick J. 1992, A&AS, 96, 26
Steffen, W., Holloway, A. J., & Pedlar, A. 1996, MNRAS, 282, 1203
Van de Steene, G. C., & Zijlstra, A. A. 1994, A&A, 108, 485